Ion Fragment Imaging of the Ion-Pair Photodissociation of CH_3Cl, CH_3Br, C_2H_5Cl, and C_2H_5Br at 118 nm

Kunihiro Suto, Yoshihiro Sato, Claire L. Reed,† Vladimir Skorokhodov, Yutaka Matsumi, and Masahiro Kawasaki*

Institute for Electronic Science, and Graduate School of Environmental Science, Hokkaido University, Sapporo 060, Japan

Received: September 19, 1996; In Final Form: November 25, 1996[⊗]

The ion-pair photodissociation $R^+ + X^-$ ($R = CH_3$, C_2H_5 and X = Cl, Br) from their respective alkyl halides has been studied using ion photofragment imaging spectroscopy at 118.27 nm. From the structure of the R^+ images a fragment total translational energy distribution and an anisotropy parameter for angular distribution were derived. The anisotropy parameter β was 1.5 ± 0.4 (CH_3Cl), 1.6 ± 0.3 (CH_3Br), 1.9 ± 0.3 (C_2H_5Cl), and 1.7 ± 0.2 (C_2H_5Br), respectively. The fraction of total energy release going into translation was found to be relatively small, 13−21% for the molecules studied. The translational energy distributions for the methyl halides are well represented by Boltzmann distributions with temperatures of 1000 K, whereas those for the ethyl halides by Gaussian distributions peaking at 5−6 kcal mol^{-1}.

Introduction

The excited electronic states of alkyl halides (RX) have attracted considerable interest since they are considered to be model molecular systems for photodissociation dynamics studies. The well-studied group of the lowest dissociative excited electronic states of alkyl halides corresponds to the A-band continuum absorption in the UV region. Higher in energy are a series of Rydberg states which derive from the excitation of the nonbonding $np\pi$ valence electron to a Rydberg orbital, so that the first Rydberg states correspond to the $(n + 1)$s and the following Rydberg series results from promotion to the $(n + 1)$p orbital.[1−3] A background absorption which underlies the structured $(n + 1)$s and $(n + 1)$p Rydberg series has been reported for CH_3Cl ($\tilde{\nu} > 80\,000$ cm^{-1}) and CH_3Br ($\tilde{\nu} > 70\,000$ cm^{-1}). This absorption can be attributed to any electronically excited valence state that has a larger equilibrium distance r_e(C−X) than that of the ion core in the Rydberg states.[4] This is a direct consequence of the higher occupancy of antibonding orbitals σ^* in the excited valence states and the essentially nonbonding character of Rydberg orbitals. One should note that similar excited valence states in the hydrogen halides or diatomic halogens are all deeply bound states of ion-pair character.[5−8]

The formation of ion pairs at energies below the ionization potential of the parent molecule has been studied for over 50 years.[9−11] In particular, ion pairs from halogen diatomics have received notable attention.[12] The excitation functions of the ions show structure in their near-threshold spectra corresponding to Rydberg states which are predissociated by ion-pair continuum states and low-lying valence states as schematically shown in Figure 1. A similar excitation scheme is also employed for ion-pair formation from halomethanes. Suzuki et al.[13] performed a negative ion mass spectrometric study of the halomethanes, CH_3X (X = F, Cl, Br). They showed that peaks in the photodissociation efficiency curves of the negative ions (X^-) could also be assigned to transitions from the ground state to various Rydberg states of the parent molecule. The spectroscopic information obtained from these curves can provide a useful insight into the nature of the excited states. However, the dynamics of the ion-pair photodissociation

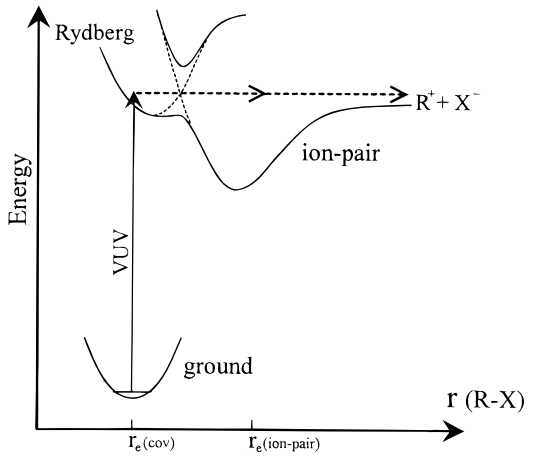

Figure 1. Photopreparation of a Rydberg state and dissociation of an ion-pair state of alkyl halides by vacuum ultraviolet excitation.

$$RX + h\nu \rightarrow R^+ + X^- \quad (1)$$

remains poorly understood. The only investigation of the ion-pair production from CH_3X (X = Cl, Br) at 118.27 nm has been reported by Munakata and Kasuya[14] using fragment translational spectroscopy. Recording the time-of-flight mass peak profiles of the CH_3^+ and X^- ions, they derived average anisotropy parameters and fragment translational energy release.

In the present study we report results of an ion imaging study on the angular and velocity distributions of the fragment ion R^+ in the photodissociation of CH_3Cl, C_2H_5Cl, CH_3Br and C_2H_5Br near 118 nm. This work has enabled a detailed study of the dynamics of ion-pair dissociation.

Experimental Section

The experimental apparatus design is similar to that reported earlier[15] and was described in detail previously.[16] A brief description of the setup is provided here. The three axes, molecular beam, laser beam, and time-of-flight mass spectrometer, are mutually orthogonal in the interaction region. The

† School of Chemistry, University of Bristol, Bristol BS8 1TS, U.K.
[⊗] Abstract published in *Advance ACS Abstracts,* January 15, 1997.

S1089-5639(96)02883-6 CCC: $14.00

molecular beam is formed by a pulsed valve, a skimmer, and a collimator. Sample gases, typically 10% diluted in Ar, are expanded with a total stagnation pressure of 760 Torr. The generated ions are accelerated to the detector chamber. To provide uniformity of electric fields in the extraction and acceleration region, guard ring electrodes are constructed. The guard system is mounted on a movable base plate to align precisely the ion source axes relative to the time-of-flight axes of the mass spectrometer. This allows us to obtain the most symmetric image possible.

A CCD camera attached with a gated image intensifier monitored the ion image on a phosphor screen through a lens. The image signal from the CCD camera is accumulated by a microcomputer. The experimental 2-D images were first filtered in the frequency domain to eliminate a striped shadow caused by the meshed electrodes and the video instrument. In the photofragment imaging experiment, the three-dimensional (3-D) distribution of the ion molecular fragments is projected onto a two-dimensional (2-D) detector. In the present study a filtered back-projection technique is used to recover a 3-D velocity distribution.[17] Using a computer with a Intel Pentium 120 MHz a calculation for a 256 × 256 frame in 8 bit scale takes 16 s. For analysis of the angular anisotropy of photofragments, instrumental resolution is severely reduced due to congestion of imaging data. No angular information can be obtained near the center of images. Resolution of a image was determined to be 12 pixels over 51 pixel/cm by measuring images of the photofragments from the photodissociation of iodine and iodochloride molecules at 304 nm.

The 355 nm output of a Nd^{3+}:YAG laser is tripled to produce VUV light at 118.27 nm by frequency tripling in Xe.[18] The 355 nm laser beam was focused with a quartz lens ($f = 15$ cm) into a tripling cell filled with Xe gas of 10−20 Torr, and the 118 nm light is then focused with a LiF lens ($f = 50$ mm at 118 nm) to the interaction region. This lens focuses the 355 nm light out of the interaction region because the focal length is 80 mm at 355 nm. No attempt is made to separate the 118 nm light from the 355 nm light.

Results

CH_3^+ cations from the photodissociation of CH_3Br in argon at 118 nm were observed in the transient TOF mass spectra. We also observed Ar^+, CH_3Br^+ and $(CH_3Br)_2^+$ ions in the TOF spectrum. The CH_3^+ ions were deduced to come from dissociation of CH_3Br ion-pair states,[14] and Ar^+ from multiphoton ionization of Ar. CH_3Br^+ comes mainly from dissociation of $(CH_3Br)_2^+$ and is discussed elsewhere.[19] None of these ions were produced when the VUV light was removed by evacuating the Xe frequency tripling cell. These results indicate no multiphoton processes by the 355 nm light. Hence, VUV light at 118 nm is the necessary factor for formation of the positive ions. Only a small portion of the CH_3Br^+ ions observed are deduced to come from hot-band VUV ionization of the parent molecule as the ionization potential of CH_3Br (10.53 eV) is slightly above the photon energy of 118.27 nm (10.483 eV).

We tested the CH_3Br concentration dependence of the various ion signals. Gas mixtures of 2.5, 5, 7.5, and 10% of the methyl bromide vapor in argon were investigated at various stagnation pressures (600−760 Torr). A log−log plot of the CH_3^+ signal intensity versus the CH_3Br^+ signal intensity gave a quadratic dependence, showing that CH_3^+ did not come directly from CH_3Br^+. The absence of the CH_3^+ signals from clusters of CH_3Br and Ar was verified by the fact that exchanging the Ar buffer gas with He gas did not change the CH_3^+ image.

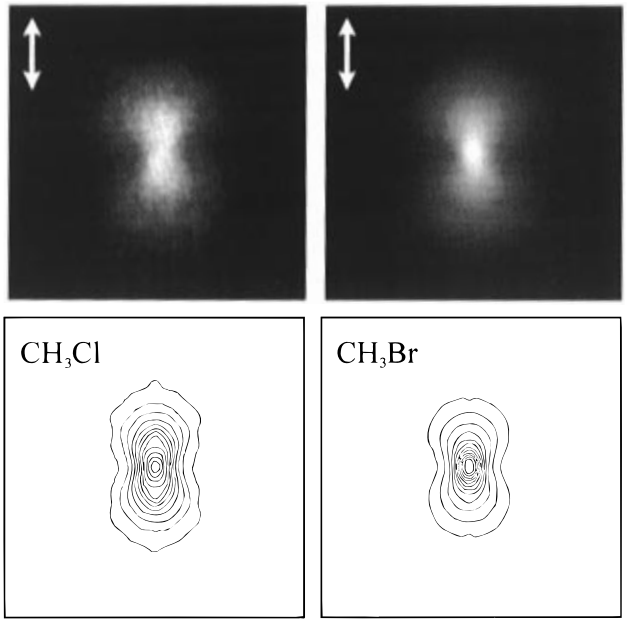

Figure 2. Images of CH_3^+ ions from the photodissociation of CH_3Cl (left) and CH_3Br (right) at $\lambda = 118.27$ nm. The electric vector of the laser beam lies in the plane as shown by an arrow. Top: 2-D images. Bottom: contour maps of the equatorial slices of back-projected 3-D images.

The 2-D raw images of CH_3^+ ions from the photodissociation of CH_3Br at 118 nm are presented in the upper panel of Figure 2, where the polarization vector of the laser light was aligned perpendicular to the detection axis and the laser light beam was polarized in the plane as shown by an arrow. We performed an analogous experiment for CH_3Cl, and its results are shown in the upper panel of Figure 2. The lower panel of each figure shows an equatorial slice of the calculated 3-D back-projected image. Reproducibility and the space-charge-induced distortion of the observed images were checked by varying the experimental conditions. Changing the RX partial pressure (2.5−10%) in the Ar-diluted gas sample and the 355 nm laser output (5−10 mJ/pulse) had no affect on the profile of the images.

The main features of the images are evident, that is, the ion intensities are mainly distributed in the outer parts of the images with strong anisotropy. We first turn our attention to analysis of the image of CH_3^+ ions observed from the photolysis of CH_3Br. In Figure 2, we notice two velocity components, one fast anisotropic velocity and the other slow isotropic velocity component. The former image is attributed to dissociation of a CH_3Br ion-pair state, whereas the latter image may be attributed to a multiphoton ionization process. Since the phospher screen has a response time of 50 ns, the signals gated typically by 100 ns could be slightly contaminated by leaked signals of other mass peaks. This could cause a centered background image.

Quantitative analyses of the images were carried out to obtain the speed and angular distributions of the alkyl ion fragments, using the back-projection method. From this back-projected image, we obtained the center-of-mass translational energy distribution and also the anisotropy parameters for the fragment angular distribution as shown in Figure 3.

The angular distribution of the fragment velocity is expressed by[20]

$$I(v,\theta) = (1/4\pi)f(v)\{1 + \beta(v)P_2(\cos\theta)\} \qquad (?)$$

where $f(v)$ is the speed distribution of the fragments, θ is the angle between the polarization vector of the photodissociation

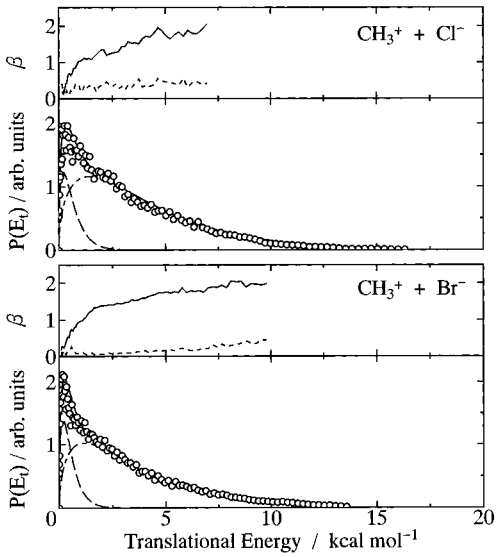

Figure 3. Dependence of the anisotropy parameter $\beta(E_t)$ on the fragment translational energy, and total translational energy distributions $P(E_t)$ in the center-of-mass frame for CH_3Cl and CH_3Br photodissociation at 118.27 nm. Broken curves in the figures of $\beta(E_t)$ show standard errors for β. Simulated Maxwell−Boltzmann functions for slow and fast components and their sum are shown. Fitting parameters are listed in Table 1.

laser light and the recoil velocity vector of the fragments, $P_2(\cos\theta)$ is the second Legendre polynomial defined as $P_2(\cos\theta) = (3\cos^2\theta - 1)/2$, and β is a spatial anisotropic parameter that ranges between −1 and 2. In the present study the speed dependence, $\beta(v)$, of the anisotropy parameter is analyzed. The obtained $\beta(E_t)$ and their standard errors are shown in Figure 3, where E_t is the fragment total translational energy in the center-of-mass frame for the dissociation process of $CH_3^+ + Br^-$. The $\beta(E_t)$ plot shows that the anisotropy parameter increases with fragment velocities. It has low positive values at low velocities and high positive values of 1.3−1.9 at high velocities.

The center-of mass translational energy distribution $P(E_t)$ is calculated from the speed distribution of the CH_3^+ fragment, $f(v)$ with an appropriate Jacobian. The thermal kinetic energy of the parent molecule is assumed to be negligible in comparison to the translational energy of the photofragments. The profile of the $P(E_t)$ distribution in this CH_3Br photodissociation implies that it can be well reproduced with a Maxwell−Boltzmann distribution at $T = 1000$ K. Other standard energy distributions, for example Gaussian or Poissonian, appear to be inappropriate. The remainder of the $P(E_t)$ distribution can be fitted with a second Maxwell−Boltzmann function at a low temperature, $T = 150$ K. This low-temperature component has a low β value close to 0 as shown in Figure 3. Overlapping of the low-temperature and high translational energy components accounts for increasing $\beta(E_t)$ values with translational energy in the low E_t region. In turn, the high translational energy component shows a rather high averaged value $\beta = 1.6 \pm 0.3$. Since the low-temperature component or the center image with $\beta \approx 0$ contributes only a little to the total CH_3^+ formation, it will not be discussed further.

Analysis of the CH_3^+ image obtained from the photodissociation of CH_3Cl gives $P(E_t)$ and $\beta(E_t)$ similar to those obtained from CH_3Br as seen in Figure 3. The translational energy distribution can again be simulated by two Boltzmann distributions with temperatures of 150 and 1000 K. The anisotropy parameter β is 0 for the low-temperature component and 1.5 ± 0.4 for the high-temperature one.

Analogous experiments were performed on C_2H_5Br and C_2H_5Cl at 118 nm. The raw images of $C_2H_5^+$ are shown in the upper panels of Figure 4. Analysis of the raw images yields equatorial slices of the 3-D velocity distributions in the lower panels of Figure 4. The center-of-mass translational energy distributions of Figure 5are approximated with a low-temperature Boltzmann component (270 K) and a Gaussian components that peaks at 6.0 kcal mol^{-1} with a fwhm of 9 kcal mol^{-1}. The anisotropy parameters obtained at high velocity region were $\beta = 1.7 \pm 0.2$ for C_2H_5Br and $\beta = 1.9 \pm 0.3$ for C_2H_5Cl. Fitting parameters are listed in Table 1.

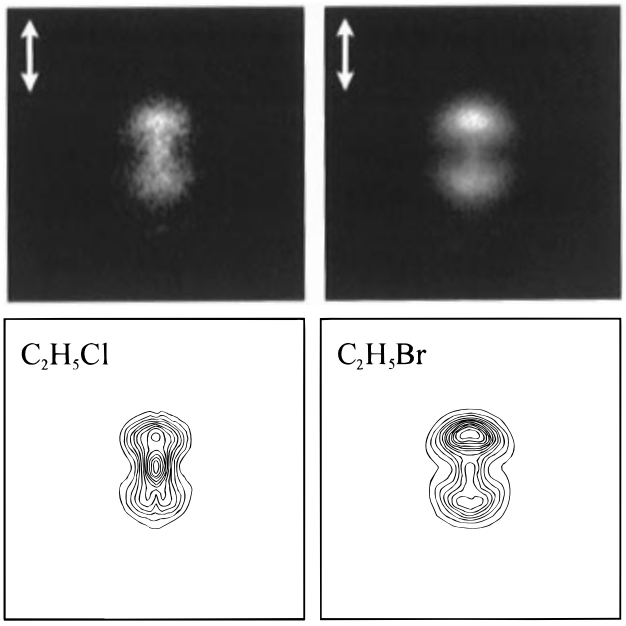

Figure 4. Images of $C_2H_5^+$ ions from the photodissociation of C_2H_5Cl (left) and C_2H_5Br (right) at 118.27 nm. See the caption of Figure 2.

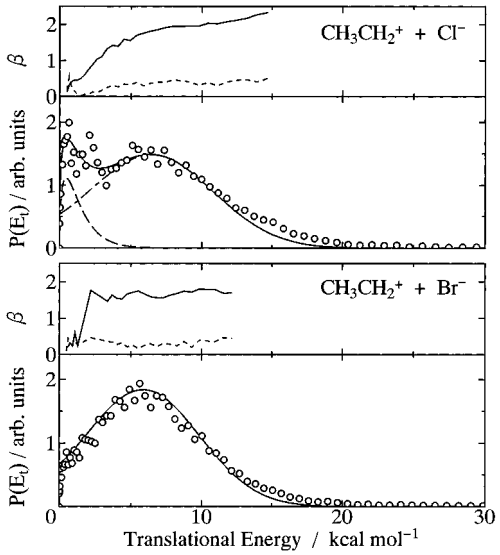

Figure 5. Dependence of the anisotropy parameter $\beta(E_t)$ on the fragment translational energy, and fragment total translational energy distributions $P(E_t)$ in the center-of-mass frame for C_2H_5Cl and C_2H_5Br photodissociation at 118.27 nm. Simulated functions for slow and fast components and their sum are shown. Fitting parameters are listed in Table 1.

When one takes a close look at the low translational energy region for C_2H_5Br in Figure 5, there is a slight contribution of the low-temperature Boltzmann component. At the low-energy region where β is close to zero, the Gaussian distribution has low translational energy and the fragment anisotropy could be smeared out by rotation of the parent molecule.

TABLE 1: Main Components of Total Translational Energy Release in the Center-of-Mass Frame for $R^+ + X^-$ Photodissociation near 118 nm[a]

RX	Maxwell−Boltzmann temp[b] (K)	Gaussian distribution (kcal mol^{-1}) peak	Gaussian distribution (kcal mol^{-1}) fwhm[c]	anisotropy parameter, β this work	anisotropy parameter, β ref 14
CH_3Cl	1000			1.5 ± 0.4	0.9 ± 0.2
CH_3Br	1000			1.6 ± 0.3	0.9 ± 0.2
C_2H_5Cl		6.0	9	1.9 ± 0.3	
C_2H_5Br		5.5	8	1.7 ± 0.2	

[a] β is derived from the high translational energy component of the $P(E_t)$ distributions. [b] Slow components or the center images are represented by the Maxwell−Boltzmann distributions with $T = 150$ K for the methyl halides and 270 K for the ethyl halides. [c] Full width at half-maximum. These values are corrected for the spectral resolution of our imaging machine.

TABLE 2: Energy Partitioning and Spatial Anisotropies of RX Ion Pair Photodissociation at 118.27 nm[a]

RX	$D_0(R^+-X^-)$	E_{avl}	$\langle E_t \rangle$	$\langle E_{int} \rangle / \langle E_{avl} \rangle$
CH_3Cl	226	16	3.0 3.9[b]	0.81
CH_3Br	217	25	3.0 3.9[b]	0.88
C_2H_5Cl	194	48	6.0	0.88
C_2H_5Br	188	54	5.5	0.90

[a] Ion pair dissociation energy $D_0(R^+-X^-)$, available energy E_{avl}, and total translational energy release $\langle E_t \rangle$ are given in kcal mol^{-1}. [b] Reference 14.

Discussion

A. Photoexcitation and Dissociation. According to photoionization studies,[11] the ion-pair dissociation of CH_3Cl occurs mainly in the limited range of photon energy from 10.0 to 13.0 eV. In addition, the VUV photon energy is lower than the ionization potentials of the CH_3Cl, CH_3Br, and C_2H_5Cl molecules and slightly exceeds that of C_2H_5Br. Therefore, ion-pair formation via the two-step excitation by 118 nm VUV absorption followed by 355 nm UV absorption can be limited. The ion-pair dissociation is induced by one-photon absorption of the ground-state CH_3Br at 118 nm. Bond dissociation energies can be estimated via ionization potentials $I_p(R)$ and $I_p(RX)$, electron affinity $E_a(X)$, and bond dissociation energy $D_0(R-X)$.[12,21,22] The derived ion pair dissociation energies are listed in Table 2,

$$D_0(R^+-X^-) = D_0(R-X) + I_p(R) - E_a(X) \qquad (3)$$

Results of a previous time-of-flight study by Munakata and Kasuya[14] for the ion-pair photodissociation of CH_3Cl and CH_3Br are also presented in Table 2. They found the time-of-flight profiles to have a strong dependence on the laser polarization and hence extracted an anisotropy parameter, $\beta = 0.9 \pm 0.2$, and translational temperatures of about 1300 K for the dissociation of both molecules. Our present results are in good agreement with their averaged values, although the present β values are higher than their values.

The β values of the high energy components of the images fall very close to the upper limiting value of 2. These high positive values of β unambiguously indicate that the ion-pair photodissociation occurs promptly following an electronic transition parallel to the R−X bond axis. Since the ground electronic state of RX molecules is $\tilde{X}^1A'$ (or $\tilde{X}^1A_1$), the pertinent electronic transition is of $^1A' \leftarrow {}^1A'$ (or $^1A_1 \leftarrow {}^1A_1$) type in the C_s (or C_{3v}) symmetry group. One can therefore expect that in each of the molecules studied, the Rydberg and, hence, ion-pair electronic state of $^1A'$ symmetry populated in the photoexcitation process correlates diabatically with the $R^+(\tilde{X}^1A') + X^-(^1S)$ dissociation limit that is involved in the observed R^+ production.

Since the dominant interaction for ion-pair states of halogen-containing molecules RX is Coulombic at large internuclear separations, these states are rather similar, having large equilibrium R−X internuclear separations (3.0−3.5 Å) and large dissociation energies (30 000−35 000 cm^{-1}).[24] The potential energy curves of these states are very wide-ranging and at shorter internuclear distances can mix with Rydberg states which can be accessed by vertical photon excitation in the Franck−Condon region as schematically shown in Figure 1. As an alternative therefore, we can imagine that after photoexcitation at 118.27 nm, above the $R^+ + X^-$ dissociation limit, the RX molecules first access Rydberg states of the $^1A'$ symmetry type (found at energies just below the ionization potential[1,3,13]) and then "cross" to ion-pair states. The dissociation pathways should cross the deep and wide attractive valley of the ion-pair state where the photoexcitation energy is channelled into internal excitation of the R^+ fragments. Note that the "crossing" must occur quickly to give the β value close to 2.[25]

B. Energy Distributions. The vibrational excitation of the fragments in the photodissociation process could be due to the optically prepared vibrational levels in the Rydberg state (Franck−Condon excitation mechanism). However, the electronic transition from a ground state of RX to a Rydberg state induces little vibrational excitation in the molecule by the Franck−Condon excitation mechanism, because photoexcitation to the Rydberg state is mostly localized in the halogen atom. Another mechanism for the vibrational excitation of photofragments is due to the repulsion force between the two fragments (impulsive excitation mechanism). Especially for the ion-pair dissociation vibrational and rotational excitation may be caused by the interaction between the X^- atom and the hydrogen atom of CH_3^+ in the ion-pair state even at a long internuclear distance (Coulomb excitation mechanism). Decomposition of RX molecules over the ion-pair surfaces is accompanied by strong coupling between the dissociative motion and other vibrational and rotational modes, resulting in high internal excitation of the R^+ fragment sharing up to 90% of the available energy. This high-energy partitioning into fragment internal excitation is in direct contrast to the low internal excitation, up to 10% of E_{avl}, in the UV photodissociation of CH_3X to $CH_3 + X$.[26,27] In the C_{3v} symmetry group the CH_3-X molecule has a symmetry axis and fragments separate in such a way that this symmetry axis is preserved, so that preferentially a_1 vibrations of the R^+ fragments can be excited. For the same symmetry preservation reasons a minor amount of the available energy should be shared by rotational degrees of freedom. This means that the symmetric bend (umbrella mode) ν_2 and the symmetric stretch ν_1 are most likely to be excited. Similar photodissociation features were observed. The absorption in the A band excites the relatively weak bound $^3Q_0^+$ or other dissociative states of the Q complex.[26] We note that the two different translational energy distributions, Gaussians for the ethyl halides and Boltzmannians for the methyl halides, reflect their different structures (bent C_s and linear C_{3v}, respectively) during diabatic dissociation via the ion-pair states. We conclude by noting that in UV dissociation of RX leading to neutral fragments gives translational energy distributions which can be characterized by a Gaussian and that have large anisotropy parameters and provides a closer fulfillment of the so-called reflection principle for the fast and direct photodissociation.

Acknowledgment. The authors thank Prof. K. Tsukiyama of The Science University of Tokyo for his suggestion of this experiment. This work is partly supported by Grants-in-Aid in Scientific Research (Y.M.) and Priority-Area-Research of "Photoreaction Dynamics" (M.K.). C.L.R. and M.K. thank the Japan−UK cooperative program supported by the Japan Society for the Promotion of Science (JSPS), The British Council, and the Royal Society for travel funds. C.L.R. also thanks the EPSRC for a studentship. V.S. thanks the JSPS fellowship.

References and Notes

(1) Truch, D. T.; Salomon, D. R.; Armstrong, D. A. *J. Mol. Spectrosc.* **1979**, *78*, 31.
(2) Baker, N. L.; Russell, B. R. *J. Mol. Spectrosc.* **1978**, *69*, 211.
(3) Causley, G. C.; Russell, B. R. *J. Chem. Phys.* **1975**, *62*, 848.
(4) Robin, M. B. *Higher Excited States of Polyatomic Molecules*; Academic Press: New York, 1974, Vol. 1; 1985, Vol. 3.
(5) Bettendorf, M.; Buenker, R. J.; Peyerimhoff, S. D.; Romelt, J. *Z. Phys. A* **1982**, *304*, 125.
(6) Green, D. S.; Wallace, S. C. *J. Chem. Phys.* **1992**, *96*, 5857.
(7) Teichteil, C.; Pelissier, M. *Chem. Phys.* **1994**, *180*, 1.
(8) Peyerimhoff, S. D.; Buenker, R. J. *Chem. Phys.* **1981**, *57*, 279.
(9) Cordes, H. *Z. Phys.* **1936**, *97*, 603.
(10) Dibeler, V. H.; Walker, J. A. *J. Chem. Phys.* **1965**, *43*, 1842.
(11) Krauss, M.; Walker, J. A.; Dibeler, H. *J. Res. Natl. Bur. Stand.* **1968**, *72A*, 281.
(12) Kaur, D.; Yencha, A. J.; Donovan, R. J.; Kvaran, A.; Hopkirk, A. *Org. Mass. Spectrom.* **1993**, *28*.
(13) Suzuki, S.; Mitsuke, K.; Imamura, T.; Koyano, I. *J. Chem. Phys.* **1992**, *96*, 7500.
(14) Munakata, T.; Kasuya, T. *Chem. Phys. Lett.* **1989**, *154*, 604.
(15) Chandler, D. W.; Houston, P. L. *J. Chem. Phys.* **1987**, *87*, 1445.
(16) Sato, Y.; Matsumi, Y.; Kawasaki, M.; Tsukiyama, K.; Bersohn, R. *J. Phys. Chem.* **1995**, *99*, 16307.
(17) Budinger, T. F.; Gullberg, G. T. *IEEE. Trans. Nucl. Sci.* **1974**, *NS-21*, 2.
(18) Hilbig, R.; Wallenstein, R. *Appl. Opt.* **1982**, *21*, 913.
(19) Suto, K.; Sato, Y.; Matsumi, Y.; Kawasaki, M. *J. Phys. Chem.*, in press.
(20) Zare, R. N.; Herschback, D. R. *Proc. IEEE* **1963**, *51*, 173.
(21) Hotop, H.; Lineberger, W. C. *J. Phys. Chem. Ref. Data* **1985**, *14*, 731.
(22) Herzberg, G. *Electronic Spectra and Electronic Structure of Polyatomic Molecules*; Van Nostrand Co.: Princeton, NJ, 1967.
(23) DeMore, W. B.; Sander, S. P.; Golden, D. M.; Hampson, R. F.; Kurylo, M. J.; Howard, C. J.; Ravishankara, A. R.; Kolb, C. E.; Molina, M. J. *JPL Publication 94-26*; Jet Propulsion Laboratory: Pasadena, CA, 1994.
(24) Brand, J. C. D.; Hoy, A. R. *Appl. Spectrosc. Rev.* **1987**, *23*, 285.
(25) Yang, Y.; Bersohn, R. *J. Chem. Phys.* **1974**, *61*, 4400.
(26) van Veen, G. N. A.; Baller, T.; de Vries, A. E. *Chem. Phys.* **1985**, *97*, 179.
(27) Loo, R. O.; Haerri, H.-P.; Hall, G. E.; Houston, P. L. *J. Chem. Phys.* **1989**, *90*, 4222.